Development of molten salt-based processes through thermodynamic evaluation assisted by machine learning

Lucien Roach, Arnaud Erriguible, Cyril Aymonier

▶ **To cite this version:**

Lucien Roach, Arnaud Erriguible, Cyril Aymonier. Development of molten salt-based processes through thermodynamic evaluation assisted by machine learning. Chemical Engineering Science, 2024, 299, pp.120433. 10.1016/j.ces.2024.120433 . hal-04650280

HAL Id: hal-04650280
https://hal.science/hal-04650280v1

Submitted on 16 Jul 2024

HAL is a multi-disciplinary open access archive for the deposit and dissemination of scientific research documents, whether they are published or not. The documents may come from teaching and research institutions in France or abroad, or from public or private research centers.

L'archive ouverte pluridisciplinaire **HAL**, est destinée au dépôt et à la diffusion de documents scientifiques de niveau recherche, publiés ou non, émanant des établissements d'enseignement et de recherche français ou étrangers, des laboratoires publics ou privés.

Distributed under a Creative Commons Attribution - NonCommercial - NoDerivatives 4.0 International License

Graphical Abstract

Development of molten salt–based processes through thermodynamic evaluation assisted by machine learning

Lucien Roach, Arnaud Erriguible, Cyril Aymonier

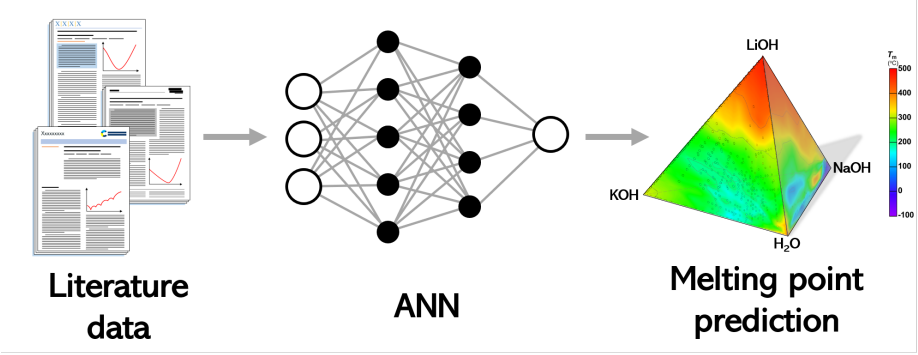

Development of molten salt–based processes through thermodynamic evaluation assisted by machine learning

Lucien Roach[a], Arnaud Erriguible[a,b], Cyril Aymonier[a,*]

[a] *Univ. Bordeaux, CNRS, Bordeaux INP, ICMCB, UMR 5026, Pessac, 33600, France*
[b] *I2M–UMR5295, Univ. Bordeaux, Bordeaux INP, CNRS, site ENSCBP, 16 avenue Pey–Berland, Pessac, 33600, France*

Abstract

Molten salt–based processes and hydrofluxes are highly sensitive to mixture composition and require knowledge of the combined melting point for successful materials syntheses. In particular processes using hydroxide–based fluxes (pure salt melts) and hydrofluxes (salt melts containing 15–50 % H_2O) have been shown to be interesting environments to synthesize inorganic materials in high oxidation states. The development of tools to predict these properties are desirable to inform the implementation of processes using these mixtures. In this work, we use an artificial neural network model to estimate the melting points of fluxes and hydrofluxes comprising of quaternary mixtures of NaOH, KOH, LiOH, and H_2O. A database of 1644 data points collected from 47 different sources was used in the training of the model. Melting points were predicted from the molar fractions of each component (4 independent variables). After training, the ANN model was able to approximate the melting points of the mixture with an R^2 of 0.996 for most conditions. Except for a region defined by the range $0.08 \lesssim \Phi_{\mathrm{LiOH}} \lesssim 0.14$ and $\Phi_{\mathrm{H_2O}} \lesssim 0.85$, where the liquidus surface was multi–valued, preventing accurate representation by the ANN. The model was able to qualitatively recreate the binary curves and ternary liquidus surfaces of these mixtures with a root mean squared error of 6.1 °C (Full range −65 – 477 °C). In the future, this model could be used to aid the synthesis of materials

*Corresponding author:
Email address: cyril.aymonier@icmcb.cnrs.fr (Cyril Aymonier)

in the quaternary mixtures investigated in this work.

Keywords: Machine Learning, Molten Salt–Based Processes, Artificial Neural Network, Melting Points, Alkali Metal Hydroxides

---

1. Introduction

Alkali metal hydroxides are interesting agents to use in the synthesis of inorganic materials, in particular as solvents in processes using molten salts (fluxes) [1–18], or alongside water in hydrofluxes [19–31]. The advent of novel liquid–liquid phase–segregated solvent systems, such as hydrothermal molten salts (HyMoS), comprised of alkali metal hydroxides and water, offer the prospect of developing these syntheses into continuous processes [32, 33]. Molten salt mixtures and hydrofluxes can be active participants in synthesis reactions and have high mass transport, allowing the creation of materials inaccessible *via* solid–state reactions controllable through the composition of the salt mixture [34, 35]. For instance, these processes have enabled the synthesis of novel inorganic materials in high oxidation states, featuring unusual cations such as pentavalent manganese [23, 36]. Compared with hydrothermal techniques, hydrofluxes allow high–temperature syntheses to be performed at low–pressure due to the strong bonding of hydroxide ions to water [37, 38]. These processes are highly sensitive to the mixture composition and consequently, the temperature required to sustain such a composition in a liquid state [39]. Beyond materials synthesis, molten mixtures of alkali metal hydroxides and water have found applications in a wide range of fields; such as high-temperature electrochemistry in fuel cells, hydrogen–production processes, and electrolyzers, [40–42] and in waste treatment [43–48]. Hence, there is a great interest in being able to adequately predict the properties of molten salt mixtures [49–51] and their mixtures with water [52–56].

The alkali metal hydroxides (Li, Na, K in this study) used in these approaches are salts with low melting points (∼320 °C, ∼410 °C, and ∼471 °C, for NaOH, KOH, and LiOH, respectively) [57–59]. These salts have high solu-

bilities in water (∼5.3, ∼25, and ∼22 M at 25 °C, 1 atm for LiOH, NaOH, and KOH, respectively) [60] and when molten, these salts are completely miscible with each other. The phase behavior below the liquidus line of alkali hydroxide – water mixtures can be quite complex, with NaOH forming eight crystalline hydrates [60–62]. Mixtures of these alkali metal hydroxides also result in eutectics (i.e., a lower melting point than either of the pure components) with melting points of ∼170 °C, ∼220 °C, and ∼218 °C for mixtures of 50:50 NaOH:KOH, 71:29 KOH:LiOH, and 71:29 NaOH:LiOH [63]. Mixtures of these salts and water also form eutectics, with melting points of −27 °C, −65 °C, −27 °C for mixtures of 18.5:91.5 NaOH:H_2O, 12.5:87.5 KOH:H_2O, and 8.3:91.7 LiOH:H_2O [60]. All of the work on the ternary and quaternary mixtures of hydroxides and water is found in journals originating in the USSR [63–89]. These works have identified a range of binary compounds forming below the liquidus surface, as well as incongruently melting ternary compounds of unknown composition [63–66].

Because of the high demand to have a solid thermodynamic understanding of these systems, several computational approaches have been proposed for the prediction of phase behavior in salt mixtures [90]. The most commonly used is CALPHAD (CALculation of PHAse Diagrams) [91–95]. Several CALPHAD software products exist that can accurately predict phase diagrams for mixtures, although the computational requirements of these calculations increase substantially with compositional complexity. CALPHAD is also highly dependent on the use of comprehensive and accurate thermodynamic databases, which are costly to access and may not exist for all materials. Calculations for a system such as the NaOH–KOH–LiOH–H_2O quaternary would require a large amount of computation time and a thermodynamic basis that is currently incomplete.

An alternative, more affordable approach to phase prediction is the use of machine learning, which can predict melting points of mixtures by capturing patterns and relationships learned from training on a data set of known compositions and melting points [96]. After training, machine learning models can make predictions in relatively short timescales making them extremely efficient tools in some applications. Machine learning models have become increasingly

prominent in the prediction of thermophysical properties of materials [90]. These have included properties such as thermal conductivities [97–99], phase equilibria [100–102], and diffusion coefficients [103–106]. While there are currently numerous examples of machine learning models predicting other properties of molten salt systems [63, 90, 107–110], or predicting phase equilibria in other single component systems [111–119], work combining these two goals are still relatively uncommon. Although work exists using machine learning to predict phase equilibria in binary systems can be found [120–122]. We found no examples of using machine learning to make predictions for ternary or higher order mixtures.

In the case of binary mixtures, Sun *et al.* used molecular properties such as the self–association constants, molecular weights, and accentricity, alongside the molar fractions and thermodynamic variables such as temperature and pressure to predict the vapor-liquid equilibria of binary mixtures using artificial neural network (ANN) and random forest models [121]. Their random forest model was less accurate than the nonrandom two-liquid model, but could be trained and make predictions rapidly. The model was however limited to two components, which makes it unsuitable for the problem we address in this study. Chen *et al.* used an ANN to predict the phase equilibria of aqueous–ionic liquid binary systems using 71 parameters describing the structure of each component [120]. Their model correlated strongly with experimental data ($R^2 = 0.92$), but again this was restricted to binary system.

In this work, we demonstrate the use of an ANN to predict the melting points of quaternary mixtures of alkali hydroxides (Li, Na, K) and water using data harvested from the literature. This model allows the prediction of composition–specific properties of hydroxide water mixtures, which is highly–desirable knowledge in the development of inorganic syntheses using molten hydroxide fluxes and hydrofluxes.

2. Methods

2.1. Data Collection and Pre–processing

Melting point, T_{m}, data for NaOH, KOH, LiOH, and H_2O; as well as for mixtures thereof was collected from the published literature. Only data that was explicitly measured experimentally was included in the dataset. Data produced by extrapolation or theoretical models were not included. In total, 1644 data points were collected from 47 different sources (50 points excluded) [57–86, 123–139]. Where compositions were given as wt. % in the sources, these were converted to mol. %, using $M_{\mathrm{W,H_2O}} = 18.022$ g·mol^{-1}, $M_{\mathrm{W,LiOH}} = 23.948$ g·mol^{-1}, $M_{\mathrm{W,NaOH}} = 39.997$ g·mol^{-1}, and $M_{\mathrm{W,KOH}} = 56.106$ g·mol^{-1} for the calculation. Melting point data in these papers was collected by variety of techniques included equilibrium solubility, calorimetry, thermography and the method of P–V curves, which mostly showed good correlation. There were some limitations to the dataset, some measurements were performed under pressure, but the pressure was not recorded or given in the relevant publication. Some points were observed to deviate strongly from the rest of the data set. These were eliminated based on the magnitude of their deviation. These data points were found in 8 papers [64, 66, 83, 127, 136, 139] (see Section S1 in the Supporting Information the full data set). The cause of the deviation is suspected to originate in water contamination of the hydroxide salts in several cases [127, 136, 139], in other cases the source of the deviation is not obvious, because the quality of these points could not be verified, they were excluded from the main dataset. [64, 66, 83] Experimental error was not reported in enough of the studies to be reliably included in our model.

The dataset was scaled using the *preprocessing.scaler* function of the *Scikit-learn* Python package. [140] This function centers and scales each data point as the number of standard deviations from its mean value in the data set (i.e., the z-score, $z = (x - \bar{x})/\sigma_x$). Finally, the data was randomly split 80 % – 20 % into a training and a testing set using the *model_selection.train_test_split* function of the *Scikit-learn* Python package with *random_state* = 3. [140] The mean

and standard deviations of the test and training sets were $T_m^{(\text{Train})} = 159.9$ °C, $\sigma_{T_m}^{(\text{Train})} = 140.6$ °C, $T_m^{(\text{Test})} = 172$ °C, and $\sigma_{T_m}^{(\text{Test})} = 133.6$ °C. All hyper–parameter optimization and validation were performed on the training set.

2.2. Machine Learning Model

The ANN used in this work was implemented using the *Scikit–learn* Python package [140]. Specifically, the *neural_ network.MLPRegressor* function. The script used to train and test the ANN is available as an iPython notebook in the Supporting Information [141]. The ANN takes four inputs Φ_{NaOH}, Φ_{KOH}, Φ_{LiOH}, and $\Phi_{\text{H}_2\text{O}}$ (molar fractions of NaOH, KOH, LiOH, and H_2O, respectively) and has a single output, T_m, the melting point of the mixture.

2.3. Cross Validation

Hyper–parameter optimization was performed through 5–fold cross–validation using the *model_ selection.GridSearchCV* function included in the *Scikit–learn* Python package [140]. Two rounds of hyper–parameter optimization were performed. First, an exhaustive search of all parameters of combinations of solvers (Adam and limited–memory Broyden–Fletcher–Goldfarb–Shanno (LBFGS)), learning rate (constant, adaptive, inverse scaling), activation functions (rectified linear unit (ReLU), Identity, Tanh, Logistic) and ANN structure (permutations of 50, 100, or 150 artificial neurons per layer in up to three layers) was performed (Table S4 in the Supporting Information). It was found that the Adam solver and the identity activation function performed poorly and changing the learning rate had little impact on the score (Figures S5 and S6).

Following this, a second round of cross–validation was performed using only the LBGFS solver and omitting the Linear activation function. The tested ANN structures consisted of permutations of 50, 100, 150, or 200 neurons per layer in up to three layers. After hyper–parameter optimization, the optimal configuration was found to be 3 hidden layers containing 100, 150, and 50 hidden neurons respectively, using the LBFGS solver and ReLU as the activation functions. Across the five folds, this configuration had the highest average $R^2 = 0.9863$ and

lowest standard deviation in the R^2, $\sigma_{R^2} = 0.009$ (Table S5 in the Supporting Information). The results of the hyper–parameter optimization are summarized in Sections S2 and S3 of the Supporting Information.

3. Results and Discussion

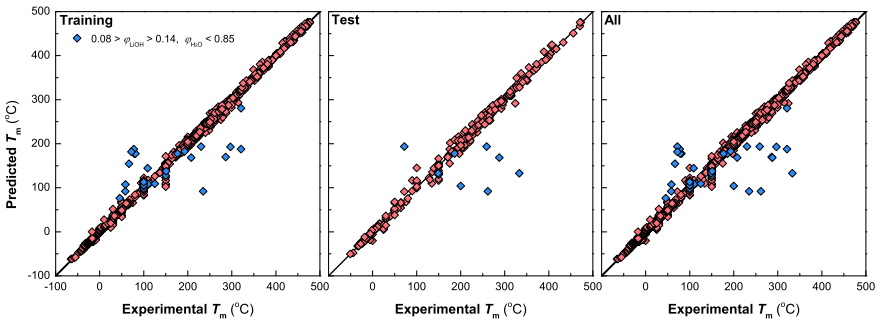

Figure 1: Published data *vs.* ANN predicted melting points for the testing, training, and entire data set. The data where $0.08 \lesssim \Phi_{\mathrm{LiOH}} \lesssim 0.14$, and $\Phi_{\mathrm{H_2O}} \lesssim 0.85$ have been highlighted in blue.

We first compiled a data set comprised of experimentally measured melting points for NaOH, KOH, LiOH, and H_2O, as well as mixtures thereof. In total, 1594 data points of acceptable quality were found in the literature. 39 of these data points covered the melting points of the isolated compounds that were collected. The points were distributed as follows: Binaries – NaOH–KOH (96 data points), KOH–LiOH (209), and NaOH–LiOH (100), NaOH–H_2O (378), KOH–H_2O (145), and LiOH–H_2O (83). Ternaries – NaOH–KOH–LiOH (271), NaOH–KOH–H_2O (54), KOH–LiOH–H_2O (87), and NaOH–LiOH–H_2O (80). NaOH–KOH–LiOH–H_2O quaternary (61). 50 points from 8 sources were rejected from the final data set because they deviated too strongly from the other data compiled [64, 66, 83, 127, 136, 139].

The full data set is available in Section S1 of the Supporting Information. The data in the binary and ternary mixtures is plotted in Figures S1-3 of the Supporting Information.

A note should be made regarding the melting point of anhydrous KOH; a wide range of melting points between 360 and 410 °C are reported in the literature, this has been noted elsewhere (i.e., Refs. [58, 142] and Table S1 in the Supporting Information). Values of ∼360 °C or ∼380 °C are commonly found in the literature, product specifications, and chemical property databases. These values are incorrect and reflect measurements taken on KOH contaminated with water. The removal of water from KOH powders is notoriously difficult. As a result, several studies reporting incorrectly low melting points for pure KOH have been published, which have unfortunately become prominent sources for $T_{\mathrm{m,KOH}}$. However, a melting point above 400 °C is more consistent with the majority of published literature on this topic (Table S1 in the Supporting Information). Seward and Martin, who corrected for the water content of their salt, found the melting point of anhydrous KOH to be (410 ± 1) °C [58]. Hence, the two studies presenting $T_{\mathrm{m}} < 400$ °C for KOH were excluded from the data set [127, 138].

The predicted *vs.* true values for the melting point of the NaOH, KOH, LiOH, and H_2O mixtures are shown in Figure 1. The trained model was able to predict the contents of the training set, testing set, and whole data set with R^2 values of 0.976, 0.883, and 0.961, respectively. These values initially seem underwhelming. However, the values that deviate strongly from the $y = x$ line, all belong to a group of data points satisfying the following criteria: $0.08 \lesssim \Phi_{\mathrm{LiOH}} \lesssim 0.14$, and $\Phi_{\mathrm{H_2O}} \lesssim 0.85$. The feature associated with this is visible in the apparent in the liquidus curves of the LiOH–H_2O binary and the NaOH–LiOH–H_2O and KOH–LiOH–H_2O ternaries. This feature will be discussed again later. Eliminating these points from the analysis (i.e., using only the red points in Figure 1) significantly improves the R^2 values to 0.9986, 0.996, and 0.998 for the training, testing, and entire data set respectively. Whereas, the excluded data points give much lower R^2 values of 0.338, −0.086, and 0.173 for the training, testing, and entire data set respectively. Hence, it is apparent that the model can estimate the majority of the data points in the data set to within a reasonable degree of accuracy, while it fails the range of mixtures where $0.08 \lesssim \Phi_{\mathrm{LiOH}} \lesssim 0.14$, and

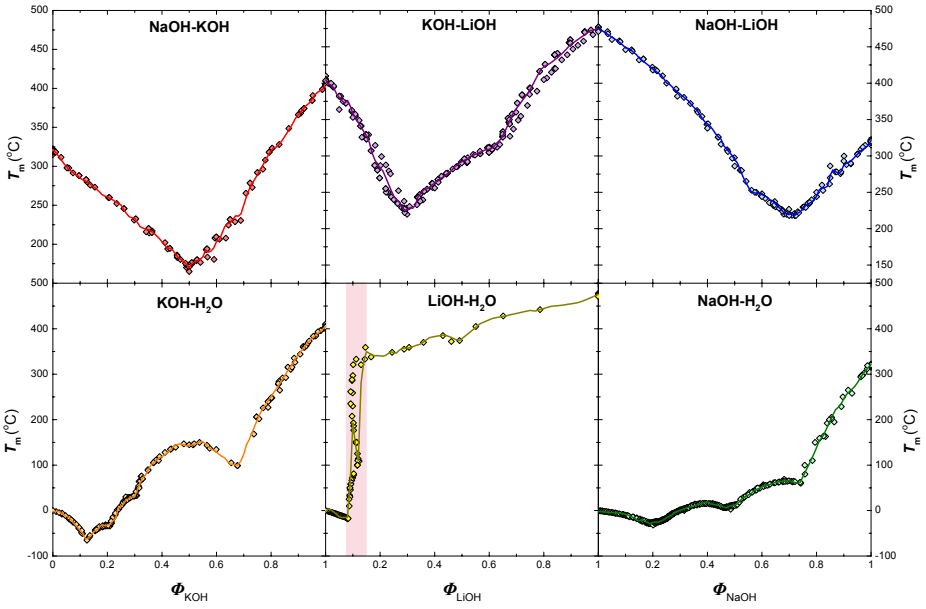

Figure 2: ANN–predicted melting points (lines) vs. published data (points) as a function of molar fraction for each of the binary compositions. The ANN model closely fits the experimental data in regions where the solid–liquid phase transition is single–valued. But fails where the phase transition is multi–valued (red region of LiOH-H_2O binary).

$\Phi_{H_2O} \lesssim 0.85$.

Finally, before inspecting the ability of the model to reflect the different binaries and ternaries in these systems, it is worth noting that the vertical linear series of points at 150 °C below the rest of the data in Figure 1 arise from the KOH–LiOH–H_2O series of a single source, it is unclear whether the data should be treated as an outlier from the rest of the data set, it has been retained in the data set [71].

By plotting the data along each of the six binaries in this system, it is possible to observe where the incorrectly predicted points emanate (Figure 2). For the NaOH–KOH, KOH–LiOH, NaOH–LiOH, NaOH–H_2O, and KOH–H_2O binaries, the collected data within experimental uncertainty is single–valued, i.e., for every combination of the independent variables (molar fractions) there is a unique corresponding value of the dependent variable (T_m). However, for the

LiOH–H_2O binary, this is not the case, the model fails in the multiply defined region of the liquidus curve ($0.08 \lesssim \Phi_{\mathrm{LiOH}} \lesssim 0.14$). The problems in this section of the curve stem from the poor solubility of LiOH compared to NaOH and KOH. The maximum solubility of LiOH in H_2O at 1 atm is $\Phi_{\mathrm{LiOH}} = 0.157$, where the boiling curve meets the liquidus curve at this concentration at $T =$ 108.9 °C [62]. The only sources for the rest of the liquidus curve were performed under pressure to increase the solubility of LiOH, but the working pressures were not specified. The only given information on the pressure conditions suggests that in the region of ($0.08 \lesssim \Phi_{\mathrm{LiOH}} \lesssim 0.14$, 270 °C $\lesssim T_{\mathrm{m}} \lesssim$ 350 °C), pressure is at maximum, with an upper limit on the pressure (due to the equipment used) of 50 MPa [62, 131]. In the range, $0.08 \lesssim \Phi_{\mathrm{LiOH}} \lesssim 0.14$, the applied pressure for $T_{\mathrm{m}} >$ 108.9 °C, results in the liquidus curve in Figure 2 appearing to be multi–valued, because a dependent variable is ignored, preventing adequate fitting in this region. This is impossible to avoid without generating significant additional data detailing the pressure dependency of the solubility of these compounds, hence the ANN model fails in this region.

For $\Phi_{\mathrm{LiOH}} \gtrsim 0.14$, measurements were still taken under pressure, but the curve is single–valued, hence the model can fit the data in this region without issue, although it is incapable of reflecting this dependency. With the exception, of the melting point of anhydrous LiOH which can be measured at atmospheric pressure and is in the range 471 – 477 °C (Table S1 in the Supporting Information). Similarly, without the acquisition and publication of significant additional data, the ANN cannot reflect the pressure dependencies at $\Phi_{\mathrm{LiOH}} \gtrsim 0.14$.

Turning to the NaOH–KOH–LiOH, KOH–LiOH–H_2O, NaOH–LiOH–H_2O, and NaOH–KOH–H_2O ternaries, which define the limits of NaOH–KOH–LiOH–H_2O system. The collected data set for these ternaries is plotted in Figures S2 and S3 of the Supporting Information, the data set has been interpolated to approximate the entirety of all the ternaries. It can be seen in the raw data set that the multi-valued region of the LiOH–H_2O binary extends into both the NaOH–LiOH–H_2O and KOH–LiOH–H_2O ternaries. This region is roughly bounded by the conditions that $0.08 \lesssim \Phi_{\mathrm{LiOH}} \lesssim 0.14$, and $\Phi_{\mathrm{H_2O}} \lesssim 0.85$, the

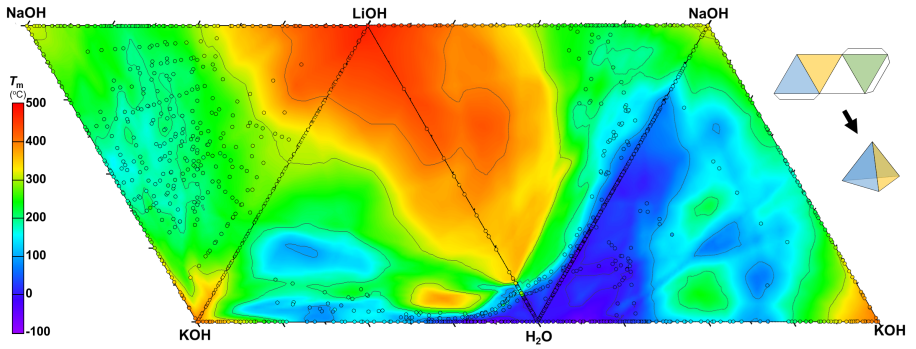

Figure 3: Map of alkali metal hydroxide ternary fluxes and hydrofluxes. Flux syntheses are typically performed in the NaOH–KOH–LiOH ternary, whereas hydrofluxes syntheses are typically performed in the region $0.15 \gtrsim \Phi_{H_2O} \gtrsim 0.55$ [25]. ANN predicted melting points for the NaOH–KOH–LiOH, KOH–LiOH–H_2O, NaOH–LiOH–H_2O, and NaOH–KOH–H_2O ternaries as a function of molar fraction of each component. Small circles indicate harvested experimental data points, and the interior color fill is matched to the reported experimental melting point. The color map indicates the output of the ANN on each ternary. Qualitatively, it can be seen that the model performs well compared with the experimental data for most compositions, as is suggested by the close match between the colors of the map and the data points. In the region, bounded by $0.08 \lesssim \Phi_{LiOH} \lesssim 0.14$, and $\Phi_{H_2O} \lesssim 0.85$, where the surface is multi–valued, it can be seen that the model is not able to reflect this feature. There are large regions in the NaOH–LiOH–H_2O and KOH–LiOH–H_2O ternaries where the model has interpolated and no experimental data exists, where assessing the accuracy of the model is difficult. Uncertainty in the experimental data is also present due to variations between sources.

data points from this region are highlighted in Figure 1.

The predictions of the trained ANN in all ternaries are shown in Figure 3. It can be seen that there is a high degree of qualitative similarity between the smoothed data set and the prediction of the ANN. The ANN fails to accurately predict the data set in the multi-valued region, where most of the points deviate strongly from the predicted surface (this is also the case for the smoothed data set). Outside of this region, the trained ANN manages to predict T_m with a root mean square error of 6.1 °C (cf. 75 °C within it) which is within the experimental error seen between the various sources comprising the data set. Unfortunately, there are not many data points for large parts of the interior regions of some of

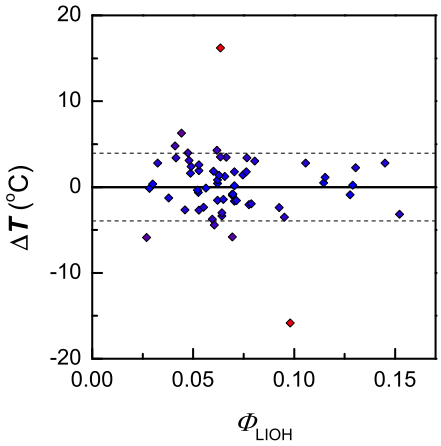

Figure 4: Absolute error in predicting the data points for the quaternary NaOH–KOH–LiOH–H_2O system at 150 °C from Itkina *et al.* [70] The dashed lines represent the range covered by root mean square error (± 3.9 °C).

the ternaries (i.e., $\Phi_{\mathrm{LiOH}} > 0.14$ for the NaOH–LiOH–H_2O and KOH–LiOH–H_2O ternaries). The ANN–predicted phase diagram is consistent with speculative phase diagrams in the literature (i.e., Refs. [65, 66, 74]). However, to the best of our knowledge, these regions remain experimentally unconfirmed.

The data for quaternary mixtures comes from a single source, Itkina *et al.* which covered a 150 °C isotherm close to the NaOH–KOH–H_2O ternary ($\Phi_{\mathrm{LiOH}} < 0.14$) [70]. We were unable to fit any other published data for the quaternary system. The trained ANN was able to predict the points from this source with root mean square error of 3.9 °C, with two clear outliers where the absolute error was above ±15 °C (Figure 4). The model performed adequately on the points available, but more data is needed to test the model further.

This model could be improved if it were extended to consider the pressure dependency of the liquidus curve. However, the limitations of the currently available data prevent this. The model could also be extended to make predictions for a broader range of salts, rather than focusing on a single quaternary system. This would include significantly expanding the data set to include other salts such as halides, nitrates, and carbonates, as well as training the model with

new inputs, beyond molar fractions. For instance, salt properties such as the atomic number, valency, and molecular weight of the anion and cation of each component; enthalpy of fusion for each component; ...etc. Such a model could potentially predict the melting points of a broad range of fluxes beyond the scope of the model presented here. Datasets like the one assembled for this study could be integrated into adaptive optimization methods to identify optimal conditions to gain information from further experimentation, such an approach could be made powerful if integrated into a self-driving robotic laboratory.

Currently, data availability acts as a bottleneck to establishing these models. Experimental data exists on a wide range of salts, but it is difficult and time–consuming to collate them into data sets, although not impossible. For instance, many of the data points used here were taken directly from Soviet–era journals. These were often difficult–to–identify and access, due to them being undigitized and untranslated. The data from these sources when located has been transcribed in the Supporting Information. However, it remains likely that further data on these systems exists in the Soviet literature that was not yet identified by us because of the language barriers and low availability of these papers. The thermophysical data available in these journals is a valuable source of training data for machine learning models, and attempts to move this data into publicly accessible databases would be beneficial to the community as a whole. Recent advances in the development of natural language processing models could help alleviate this problem by allowing the automatic extraction of this information from published papers in a range of languages. However, the success of this approach is currently limited by the lack of digitization of many of the relevant data sources.

4. Conclusion

In this paper, we have demonstrated a neural network model for the prediction of the melting points of quaternary mixtures of NaOH, KOH, LiOH, and H_2O which can be used to find the melting point of alkali metal hydroxide

fluxes and hydrofluxes for inorganic crystallite syntheses. After training with literature data, our ANN model was able to approximate the testing set with an R^2 of 0.996, excluding points in the range $0.08 \lesssim \Phi_{\mathrm{LiOH}} \lesssim 0.14$. The R^2 of the entire testing set was worse (0.883) due to a multi–valued region in this range which could not be modeled by the ANN. This feature originates from the need to pressurize LiOH solutions to maintain stability above $\Phi_{\mathrm{LiOH}} = 0.157$. However, this pressure data is currently absent from the existing literature, making it impossible to account for without further experimentation. The model was able to qualitatively recreate the binary and ternary liquidus curves of these mixtures with a root mean squared error of 6.1 °C. This model and its outputs will hopefully act as a useful tool for researchers performing syntheses in alkali metal hydroxide fluxes and hydrofluxes, by identifying the temperature conditions required to use compositions with a desired set of chemical properties. Tools like the one discussed in this study could help enable the use of quaternary mixtures to be used more reliably in the hydroflux synthesis of novel materials. Models like the one demonstrated in this study can rapidly predict phase-equilibria and could be integrated into modeling software to avoid wasting expensive computation time on thermodynamic calculations. They can also be used as tools by researchers to predict phase equilibria for molten salt and hydroflux based processes.

Declaration of Competing Interest

The authors declare that they have no known competing financial interests or personal relationships that could have appeared to influence the work reported in this paper.

Data Availability

The data set, scripts, and data generated during the preparation of this paper have been made available in the Supporting Information. These are also available through the Zenodo repository (doi.org/10.5281/zenodo.XXX).

Acknowledgments

This work was funded by the *Agence Nationale de la Recherche* (ANR, Grant No. ANR–21–CE50–0021) for financial support during the writing of this manuscript. We would like to thank Stéphane Toulin (*Institut de Chimie de la Matière Condensée de Bordeaux* (ICMCB), Bordeaux, France) for his help in obtaining the source material for many of the publications in the data set. We would also like to thank Arnault Lassin (*Bureau de Recherches Géologiques et Minières* (BRGM), Orléans, France) and Alexey Kiverin (Joint Institute for High Temperatures of the Russian Academy of Sciences (JIHT), Moscow, Russia) for their help in obtaining materials from other Soviet sources. Finally, we would also like to thank Gian–Marco Rignanese for his useful discussions during the preparation of this manuscript.

CRediT Author Statement

All authors of this paper were involved in the conceptualization of this paper and the development of the methodology. LR was responsible for the software implementation, validation, formal analysis, investigation, data curation, visualization, and writing of the original draft. All authors were involved in the review and editing of the final manuscript. AE and CA provided supervision. CA was responsible for project administration and funding acquisition.

Abbreviations

ANN	Artificial neural network
CALPHAD	CALculation of PHAse Diagrams
LBFGS	Limited-memory Broyden–Fletcher–Goldfarb–Shanno
ReLU	Rectified linear unit

References

[1] D. Wang, J. Chu, J. Li, T. Qi, W. Wang, Anti–caking in the production of titanium dioxide using low–grade titanium slag *via* the NaOH molten salt method, Powder Technol. 232 (2012) 99. doi:10.1016/j.powtec.2012.07.048.

[2] V. Srivastava, V. Kamysbayev, L. Hong, E. Dunietz, R. F. Klie, D. V. Talapin, Colloidal chemistry in molten salts: Synthesis of luminescent $In_{1-x}Ga_xP$ and $In_{1-x}Ga_xAs$ quantum dots, J. Am. Chem. Soc. 140 (2018) 12144. doi:10.1021/jacs.8b06971.

[3] C. Hu, Y. Xi, H. Liu, Z. L. Wang, Composite-hydroxide-mediated approach as a general methodology for synthesizing nanostructures, J. Mater. Chem. 19 (2009) 858. doi:10.1039/B816304A.

[4] H. Liu, C. Hu, Z. L. Wang, Composite-hydroxide-mediated approach for the synthesis of nanostructures of complex functional-oxides, Nano Lett. 6 (2006) 1535. doi:10.1021/nl061253e.

[5] J. Lee, G. F. Holland, Identification of a new strontium Ni(III) oxide prepared in molten hydroxides, J. Solid State Chem. 93 (1991) 267. doi:10.1016/0022-4596(91)90299-W.

[6] C. G. Hu, H. Liu, W. T. Dong, Y. Y. Zhang, G. Bao, C. S. Lao, Z. L. Wang, $La(OH)_3$ and La_2O_3 nanobelts – Synthesis and physical properties, Adv. Mater. 19 (2007) 470. doi:10.1002/adma.200601300.

[7] T. Minakawa, M. Kato, T. Noji, Y. Koike, Low-temperature synthesis of (Ba, K, Rb)BiO_3 using molten hydroxides, Physica C 468 (2008) 1132. doi:10.1016/j.physc.2008.05.016.

[8] T. Lusiola, F. Bortolani, Q. Zhang, R. Dorey, Molten hydroxide synthesis as an alternative to molten salt synthesis for producing $K_{0.5}Na_{0.5}NbO_3$ lead–free ceramics, J. Mater. Sci. 47 (2012) 1938. doi:10.1007/s10853-011-5984-8.

[9] M. Xu, F. Wang, M. Zhao, S. Yang, X. Song, Molten hydroxides synthesis of hierarchical cobalt oxide nanostructure and its application as anode material for lithium ion batteries, Electrochim. Acta 56 (2011) 4876. doi:10.1016/j.electacta.2011.03.027.

[10] H. Chen, C. P. Grey, Molten salt synthesis and high rate performance of the "desert–rose" form of $LiCoO_2$, Adv. Mater. 20 (2008) 2206. doi:10.1002/adma.200702655.

[11] P. Afanasiev, Molten salt synthesis of barium molybdate and tungstate microcrystals, Mater. Lett. 61 (2007) 4622. doi:10.1016/j.matlet.2007.02.061.

[12] X. Li, C. Hu, X. Wang, Y. Xi, Photocatalytic activity of CdS nanoparticles synthesized by a facile composite molten salt method, Appl. Surf. Sci. 258 (2012) 4370. doi:10.1016/j.apsusc.2011.12.116.

[13] L. Wang, K. F. Cai, Y. Y. Wang, J. L. Yin, H. Li, C. W. Zhou, Preparation and characterization of tetragonal–ZrO_2 nanopowders by a molten hydroxides method, Ceram. Int. 35 (2009) 2499. doi:10.1016/j.ceramint.2008.11.034.

[14] B. Wan, C. Hu, B. Feng, Y. Xi, X. He, Synthesis and thermoelectric properties of PbTe nanorods and microcubes, Mater. Sci. Eng., B 163 (2009) 57. doi:10.1016/j.mseb.2009.05.004.

[15] Y. Zhang, C. Hu, C. Zheng, Y. Xi, B. Wan, Synthesis and thermoelectric property of $Cu_{2-x}Se$ nanowires, J. Phys. Chem. C 114 (2010) 14849. doi:10.1021/jp105592d.

[16] Z. Zhang, C. Hu, Y. Xiong, R. Yang, Z. L. Wang, Synthesis of Ba-doped CeO_2 nanowires and their application as humidity sensors, Nanotechnology 18 (2007) 465504. doi:10.1088/0957-4484/18/46/465504.

[17] X. Wang, C. Hu, H. Liu, G. Du, X. He, Y. Xi, Synthesis of CuO nanostructures and their application for nonenzymatic glucose sensing, Sens. Actuators, B 144 (1) (2010) 220. doi:10.1016/j.snb.2009.09.067.

[18] C. Hu, W. Yan, B. Wan, K. Zhang, Y. Zhang, Y. Tian, Water-induced structure phase transition of CdSe nanocrystals in composite hydroxide melts, Physica E 42 (2010) 1790. doi:10.1016/j.physe.2010.01.050.

[19] A. M. Latshaw, W. M. Chance, N. Trenor, G. Morrison, M. D. Smith, J. Yeon, D. E. Williams, H.-C. zur Loye, $A_5RE_4X[TO_4]_4$ crystal growth and photoluminescence. Hydroflux synthesis of sodium rare earth silicate hydroxides, CrystEngComm 17 (2015) 4691. doi:10.1039/C5CE00630A.

[20] W. M. Chance, D. E. Bugaris, A. S. Sefat, H.-C. zur Loye, Crystal growth of new hexahydroxometallates using a hydroflux, Inorg. Chem. 52 (20) (2013) 11723. doi:10.1021/ic400910g.

[21] B. Tangeysh, C. Palmer, H. Metiu, M. J. Gordon, E. W. McFarland, High-temperature heterogeneous catalysis in platinum nanoparticle – Molten salt suspensions, Catal. Sci. Technol. 10 (2020) 625. doi:10.1039/C9CY01823A.

[22] D. E. Bugaris, M. D. Smith, H.-C. zur Loye, Hydroflux crystal growth of platinum group metal hydroxides: $Sr_6NaPd_2(OH)_{17}$, $Li_2Pt(OH)_6$, $Na_2Pt(OH)_6$, $Sr_2Pt(OH)_8$, and $Ba_2Pt(OH)_8$, Inorg. Chem. 52 (2013) 3836. doi:10.1021/ic302439b.

[23] R. Albrecht, T. Doert, M. Ruck, Hydroflux synthesis and characterization of the non–centrosymmetric oxomanganate(V) $KSrMnO_4$, Z. Anorg. Allg. Chem 646 (2020) 1389. doi:10.1002/zaac.202000065.

[24] A. M. Latshaw, M. D. Smith, W. M. Chance, H.-C. zur Loye, Hydroflux synthesis and crystal structure of new lanthanide tungstate oxyhydroxides, Solid State Sci. 42 (2015) 14. doi:10.1016/j.solidstatesciences.2015.03.003.

[25] M. W. Chance, Hydroflux Synthesis: A New and Effective Technique for Exploratory Crystal Growth, Ph.D., University of South Carolina, `scholarcommons.sc.edu/etd/2641/` (2014).

[26] A. M. Latshaw, B. O. Wilkins, W. M. Chance, M. D. Smith, H.-C. zur Loye, Influence of rare earth cation size on the crystal structure in rare earth silicates, $Na_2RESiO_4(OH)$ (RE = Sc, Yb) and $NaRESiO_4$ (RE = La, Yb), Solid State Sci. 51 (2016) 59. doi:10.1016/j.solidstatesciences.2015.11.009.

[27] A. J. Fernández-Carrión, M. Ocaña, J. García-Sevillano, E. Cantelar, A. I. Becerro, New single–phase, white–light–emitting phosphors based on δ-$Gd_2Si_2O_7$ for solid–state lighting, J. Phys. Chem. C 118 (2014) 18035. doi:10.1021/jp505524g.

[28] D. Ananias, F. A. A. Paz, D. S. Yufit, L. D. Carlos, J. Rocha, Photoluminescent thermometer based on a phase–transition lanthanide silicate with unusual structural disorder, J. Am. Chem. Soc. 137 (2015) 3051. doi:10.1021/ja512745y.

[29] A. M. Latshaw, W. M. Chance, G. Morrison, K. D. zur Loye, B. O. Wilkins, M. D. Smith, P. S. Whitfield, M. J. Kirkham, S. A. Stoian, H.-C. zur Loye, Synthesis of a ferrolite: A zeolitic all–iron framework, Angew. Chem. Int. Ed. 55 (2016) 13195. doi:10.1002/anie.201607800.

[30] K. D. zur Loye, W. M. Chance, J. Yeon, H.-C. zur Loye, Synthesis, crystal structure, and magnetic properties of the oxometallates $KBaMnO_4$ and $KBaAsO_4$, Solid State Sci. 37 (2014) 86. doi:10.1016/j.solidstatesciences.2014.08.013.

[31] W. M. Chance, H.-C. zur Loye, Synthesis, structure, and optical properties of a series of quaternary oxides, $K_2Ba(MO_4)_2$ (M = Cr, Mo, W), Solid State Sci. 28 (2014) 90. doi:10.1016/j.solidstatesciences.2013.12.013.

[32] T. Voisin, A. Erriguible, C. Aymonier, A new solvent system: Hydrothermal molten salt, Sci. Adv. 6 (2020) eaaz7770. doi:10.1126/sciadv.aaz7770.

[33] E. Duverger-Nédellec, T. Voisin, A. Erriguible, C. Aymonier, Unveiling the

complexity of salt(s) in water under transcritical conditions, J. Supercrit. Fluids 165 (2020) 104977.

[34] D. Portehault, I. Gómez-Recio, M. A. Baron, V. Musumeci, C. Aymonier, V. Rouchon, Y. L. Godec, Geoinspired syntheses of materials and nanomaterials, Chem. Soc. Rev. 51 (2022) 4828. doi:10.1039/D0CS01283A.

[35] D. E. Bugaris, H.-C. zur Loye, Materials discovery by flux crystal growth: Quaternary and higher order oxides, Angew. Chem., Int. Ed. 51 (2012) 3780. doi:10.1002/anie.201102676.

[36] A. Varela, I. Gómez-Recio, L. Serrador, M. Hernando, E. Matesanz, A. Torres-Pardo, M. T. Fernández-Díaz, J. L. Martínez, F. Gonell, G. Rousse, C. Sanchez, C. Laberty-Robert, D. Portehault, J. M. González-Calbet, M. Parras, Hydroxyapatites as versatile inorganic hosts of unusual pentavalent manganese cations, Chem. Mater. 32 (2020) 10584. doi:10.1021/acs.chemmater.0c03673.

[37] O. I. Martynova, V. I. Androsov, V. V. Vospennikov, Thermodynamic properties of the sodium hydroxide– water system., Reviews of Thermophysical Properties of Substance 4 (36) (1982) 4.

[38] H. He, Y. Li, R. Albrecht, M. Ruck, Oxohydroxo–tellurates(VI) $K_2[TeO_2(OH)_4]$ and $K_2[Fe_2TeO_6(OH)_2]\cdot 2H_2O$ from alkaline hydroflux, Z. Anorg. Allg. Chem. 649 (2023) 202300170. doi:10.1002/zaac.202300170.

[39] R. Albrecht, F. Graßme, T. Doert, M. Ruck, Hydroflux syntheses and crystal structures of hydrogarnets $Ba_3[RE(OH)_6]_2$ (RE = Sc, Y, Ho–Lu), Z. Naturforsch. B 75 (2020) 951. doi:10.1515/znb-2020-0147.

[40] E. Gürbüz, E. Grépin, A. Ringuedé, V. Lair, M. Cassir, Significance of molten hydroxides with or without molten carbonates in high–temperature electrochemical devices, Front. Energy Res. 9 (2021). doi:10.3389/fenrg.2021.666165/full.

[41] S. Licht, S. Liu, B. Cui, J. Lau, L. Hu, J. Stuart, B. Wang, O. El-Ghazawi, F.-F. Li, Comparison of alternative molten electrolytes for water splitting to generate hydrogen fuel, J. Electrochem. Soc. 163 (2016) 1162. doi:10.1149/2.0561610jes.

[42] J. Yang, H. Muroyama, T. Matsui, K. Eguchi, Development of a direct ammonia-fueled molten hydroxide fuel cell, J. Power Sources 245 (2014) 277. doi:10.1016/j.jpowsour.2013.06.143.

[43] M. Yu, G. Mei, X. Chen, Recovering rare earths and aluminum from waste $BaMgAl_{10}O_{17}$:Eu^{2+} and $CeMgAl_{11}O_{19}$:Tb^{3+} phosphors using NaOH sub-molten salt method, Miner. Eng. 117 (2018) 1. doi:10.1016/j.mineng.2017.12.001.

[44] F. Lecomte, A. G. P. Guiterrez, M. Huvé, A. Moissette, G. Sicoli, A.-L. Rollet, S. Daviero-Minaud, Degradation mechanisms of organic compounds in molten hydroxide salts: a radical reaction yielding H_2 and graphite, RSC Adv. 13 (2023) 19955. doi:10.1039/D3RA02537C.

[45] H. Mori, Extraction of silicon dioxide from waste colored glasses by alkali fusion using potassium hydroxide, J. Mater. Sci. 38 (2003) 3461. doi:10.1023/A:1025100901693.

[46] L. Flandinet, F. Tedjar, V. Ghetta, J. Fouletier, Metals recovering from waste printed circuit boards (WPCBs) using molten salts, J. Hazard. Mater. 213 (2012) 485. doi:10.1016/j.jhazmat.2012.02.037.

[47] S. Dai, Y. Zheng, Y. Zhao, Y. Chen, D. Niu, Molten hydroxide for detoxification of chlorine-containing waste: Unraveling chlorine retention efficiency and chlorine salt enrichment, J. Environ. Sci. 82 (2019) 192. doi:10.1016/j.jes.2019.03.007.

[48] B. M. Warnes, J. E. Schilbe, Molten metal hydroxide removal of thermal barrier coatings, Surf. Coat. Technol. 146 (2001) 147. doi:10.1016/S0257-8972(01)01370-6.

[49] C. Agca, J. W. McMurray, Empirical estimation of densities in NaCl–KCl–UCl_3 and NaCl–KCl–YCl_3 molten salts using Redlich–Kister expansion, Chem. Eng. Sci. 247 (2022) 117086. doi:10.1016/j.ces.2021.117086.

[50] A. Birri, R. Gallagher, C. Agca, J. McMurray, N. Dianne Bull Ezell, Application of the Redlich–Kister expansion for estimating the density of molten fluoride psuedo–ternary salt systems of nuclear industry interest, Chem. Eng. Sci. 260 (2022) 117954. doi:10.1016/j.ces.2022.117954.

[51] E. Cervi, S. Lorenzi, A. Cammi, L. Luzzi, Development of a multiphysics model for the study of fuel compressibility effects in the molten salt fast reactor, Chem. Eng. Sci. 193 (2019) 379. doi:10.1016/j.ces.2018.09.025.

[52] S. Gondal, H. F. Svendsen, H. K. Knuutila, Activity based kinetics of CO_2–OH^- systems with Li^+, Na^+ and K^+ counter–ions, Chem. Eng. Sci. 151 (2016) 1. doi:10.1016/j.ces.2016.05.009.

[53] S. Gondal, N. Asif, H. F. Svendsen, H. Knuutila, Density and n_2o solubility of aqueous hydroxide and carbonate solutions in the temperature range from 25 to 80 °c, Chem. Eng. Sci. 122 (2015) 307. doi:10.1016/j.ces.2014.09.016.

[54] S. Gondal, N. Asif, H. F. Svendsen, H. Knuutila, Kinetics of the absorption of carbon dioxide into aqueous hydroxides of lithium, sodium and potassium and blends of hydroxides and carbonates, Chem. Eng. Sci. 123 (2015) 487. doi:10.1016/j.ces.2014.10.038.

[55] A. Roosta, N. Rezaei, Modification of e–CPA for estimating phase equilibria and development of predictive models for electrical conductivity in aqueous electrolyte solutions, Chem. Eng. Sci. 284 (2024) 119481. doi:https://doi.org/10.1016/j.ces.2023.119481.

[56] R. Pohorecki, W. Moniuk, Kinetics of reaction between carbon dioxide and hydroxyl ions in aqueous electrolyte solutions, Chem. Eng. Sci. 43 (1988) 1677. doi:10.1016/0009-2509(88)85159-5.

[57] T. B. Douglas, J. L. Dever, Anhydrous sodium hydroxide: the heat content from 0 to 700 °C, the transition temperature, and the melting point, J. Res. Nat. Bur. Stand. USA 53 (1954) 81. doi:10.6028/jres.053.010.

[58] R. P. Seward, K. E. Martin, The melting point of potassium hydroxide, J. Am. Chem. Soc. 71 (1949) 3564. doi:10.1021/ja01178a530.

[59] C. J. Barton, J. P. Blakely, L. M. Bratcher, W. R. Grimes, The system LiOH–KOH, in: R. E. Thoma (Ed.), Phase Diagrams of Nuclear Reactor Materials, 15th Edition, Vol. ORNL-2548, Oak Ridge National Laboratory, Oak Ridge, TN, 1959, p. 141. doi:10.2172/4234144.

[60] S. U. Pickering, The hydrates of sodium, potassium, and lithium hydroxides, J. Chem. Soc., Trans. 63 (1893) 890. doi:10.1039/CT8936300890.

[61] A. v. Antropoff, W. Sommer, Das räumliche Diagramm des Dreistoffsystems NaOH–NaCl–H_2O, Z. Phys. Chem. 123U (1) (1926) 161. doi:10.1515/zpch-1926-12311.

[62] A.-P. Rollet, R. Cohen-Adad, Les systèmes « eau-hydroxyde alkalin », Rev. Chim. Minér. 1 (1964) 451.

[63] N. A. Reshetnikov, N. I. Vilutis, Ternary system of the hydroxides of lithium, sodium, and potassium, Russ. J. Inorg. Chem. 4 (1959) 123.

[64] L. S. Itkina, N. M. Chaplygina, S. M. Portnova, Formation of compounds between lithium and sodium hydroxides, Russ. J. Inorg. Chem. 14 (12) (1969) 1783.

[65] S. M. Portnova, L. S. Itkina, Solubility polytherm of the KOH-NaOH-H_2O system, Russ. J. Inorg. Chem. 14 (8) (1969) 1148, data in Abutkova 1973.

[66] L. S. Itkina, N. M. Chaplygina, S. M. Portnova, Solubility polytherm of the KOH–LiOH–H_2O system, Russ. J. Inorg. Chem. 12 (2) (1967) 282.

[67] L. S. Itkina, S. E. Ostrovityanova, Solubility polytherm of the LiOH–RbOH–H_2O System, Russ. J. Inorg. Chem. 14 (7) (1969) 1014.

[68] L. S. Itkina, N. M. Chaplygina, Solubility isotherm in the $2Li^+$, $2Na^+$ || ${CO_3}^{2+}$, $2OH^-$ – H_2O system at 50°C, Russ. J. Inorg. Chem. 8 (6) (1963) 768.

[69] L. S. Itkina, N. M. Chaplygina, S. M. Portnova, The $2Li^+$, $2Na^+$ || $2OH^-$, ${CO_3}^{2+}$ + H_2O system at 100°C, Russ. J. Inorg. Chem. 11 (4) (1966) 472.

[70] L. S. Itkina, S. M. Portnova, The KOH–LiOH–NaOH system at 150°C, Russ. J. Inorg. Chem. 12 (2) (1967) 1468, data in Abutkova 1973.

[71] L. S. Itkina, S. M. Portnova, N. M. Chaplygina, The LiOH–NaOH–H_2O and KOH–LiOH–H_2O systems at 150°C, Russ. J. Inorg. Chem. 13 (5) (1968) 740.

[72] S. M. Portnova, [*Title unknown, data reported in Itkina 1973*], Ph. D., Inst. Org. Chem. USSR Acad. Sci., Moscow, Russia (1969).

[73] S. M. Portnova, L. S. Itkina, The KOH–NaOH–H_2O system at 150°C, Russ. J. Inorg. Chem. 14 (1) (1969) 137.

[74] L. S. Itkina, Hydroxides of Lithium, Rubidium and Cesium, Nauka, Moscow, USSR, 1973.

[75] N. A. Reshetnikov, G. M. Unzhakov, [*Title unknown, data reported in Itkina 1973*], Zh. Neorg. Khim. 6 (1958) 1433.

[76] N. S. Kurnakov, V. I. Nikolaev, [*Title unknown, data reported in Itkina 1973*], Zh. Russkogo Fiz.–Khim. 58 (1926) 549.

[77] M. I. Ravich, V. I. Ketkovich, I. S. Rassonskaya, [*Title unknown, data reported in Itkina, Chaplygina, & Portnova, 1969*], Izv. Sektora Fiz.–Khim. Anal. 17 (1949) 254.

[78] N. A. Reshetnikov, G. M. Unzhakov, Thermographic investigation of binary systems of potassium and sodium hydroxides and potassium and lithium hydroxides, Iz. Fiz.–Khim. Nauch.–Issled. Inst. Irkutsk. Gosudarst Univ 2 (1) (1953) 5.

[79] N. A. Reshetnikov, G. M. Unzhakov, Irreversible reciprocal system of lithium and potassium bromides and hydroxides, Iz. Fiz.–Khim. Nauch.–Issled. Inst. Irkutsk. Gosudarst Univ 2 (1953) 23.

[80] O. Evteeva, [Title unknown, data reported in Abutkova et al. 1973, Vol 1], Izv. Sib. Otd. Akad. Nauk. SSSR Ser. Khim. Nauk., 7 (2) (1965) 144, [Data reported in: Abutkova 1973].

[81] A. B. Zdanovsky, Handbook of Solubility of Salt Systems, Vol. III., Goskhimizdat, Moscow, USSR, 1961.

[82] G. G. Diogenov, Mutually irreversible system of hydroxides and nitrates of lithium and sodium, Dokl. Akad. Nauk SSSR 89 (1953) 305.

[83] G. G. Babayan, E. B. Oganesyan, A. P. Gyunashyan, E. A. Sayamyan, [*Title unknown, data reported in Abutkova 1973, Vol. 1*], Izv. Akad. Nauk. Arm. SSR Ser. Khim. Nauk. 16 (6) (1963) 540, data reported in: Abutkova 1973.

[84] A. G. Morachevskii, N. I. Berdichevskii, Equilibria involving alkali metals and their compounds. 4. Fusibility diagrams of a potassium, sodium hydroxide, chloride, ternary reciprocal system, Zh. Prikl. Khim. 41 (1968) 732.

[85] N. A. Reshetnikov, O. G. Perfil'eva, Phase transformations in the Ki, Li || CO_3, OH ternary recipricol system, Russ. J. Inorg. Chem. 13 (5) (1968).

[86] G. M. Unzhakov, Reciprocal system of potassium and lithium hydroxides and chloride, Dokl. Akad. Nauk SSSR 87 (5) (1952) 791.

[87] L. M. Abutkova, A. B. Zdanovsky, E. I. Lyakhovskaya, E. F. Solovyeva, N. E. Shestakov, R. E. Shleimovich, Experimental Solubility Data on Salt–Water Systems. Vol. 1 – Three Component Systems, 2nd Edition, "Chemistry" Publishing, Leningrad, USSR, 1973.

[88] L. M. Abutkova, A. B. Zdanovsky, E. I. Lyakhovskaya, E. F. Solovyeva, N. E. Shestakov, R. E. Shleimovich, Experimental Solubility Data on Salt–Water Systems. Vol. 2 – Four–component and more complex systems, 2nd Edition, "Chemistry" Publishing, Leningrad, USSR, 1975.

[89] A. T. Nizhnik, A. A. Lastochkina, Thermal study of the caustic potash – water system., Ukr. Khim. Zh. 18 (1952) 397.

[90] T. Porter, M. M. Vaka, P. Steenblik, D. Della Corte, Computational methods to simulate molten salt thermophysical properties, Commun. Chem 5 (1) (2022) 1. doi:10.1038/s42004-022-00684-6.

[91] P. J. Spencer, A brief history of CALPHAD, Calphad 32 (1) (2008) 1. doi:10.1016/j.calphad.2007.10.001.

[92] W. J. Ng, H. J. Ryu, Effects of base salt additives on NaCl–UCl_3–$PuCl_3$ fuel systems: Insights from CALPHAD simulations, J. Mol. Liq. 379 (2023) 121649. doi:10.1016/j.molliq.2023.121649.

[93] V. R. Manga, S. Bringuier, J. Paul, S. Jayaraman, P. Lucas, P. Deymier, K. Muralidharan, Molecular dynamics simulations and thermodynamic modeling of NaCl–KCl–$ZnCl_2$ ternary system, Calphad 46 (2014) 176. doi:10.1016/j.calphad.2014.04.004.

[94] S. Fujiwara, M. Inaba, A. Tasaka, New molten salt systems for high-temperature molten salt batteries: LiF–LiCl–LiBr-based quaternary systems, J. Power Sources 195 (2010) 7691. doi:10.1016/j.jpowsour.2010.05.032.

[95] L. Hao, S. Sridar, W. Xiong, Thermodynamic description of molten salt systems: KCl-LiCl-NaCl and KCl-LiCl-$NdCl_3$, J. Mol. Liq. 382 (2023) 121869. doi:10.1016/j.molliq.2023.121869.

[96] G. Deffrennes, K. Terayama, T. Abe, E. Ogamino, R. Tamura, A framework to predict binary liquidus by combining machine learning and CALPHAD assessments, Mater. Des. 232 (2023) 112111. doi:10.1016/j.matdes.2023.112111.

[97] R. Shams, S. Esmaili, S. Rashid, M. Suleymani, An intelligent modeling approach for prediction of thermal conductivity of CO_2, J. Nat. Gas Sci. Eng. 27 (2015) 138. doi:10.1016/j.jngse.2015.08.050.

[98] M. Nait Amar, A. Jahanbani Ghahfarokhi, N. Zeraibi, Predicting thermal conductivity of carbon dioxide using group of data-driven models, J. Taiwan Inst. Chem. Eng. 113 (2020) 165. doi:10.1016/j.jtice.2020.08.001.

[99] A. Tatar, A. Barati-Harooni, A. Najafi-Marghmaleki, B. Norouzi-Farimani, A. H. Mohammadi, Predictive model based on ANFIS for estimation of thermal conductivity of carbon dioxide, J. Mol. Liq. 224 (2016) 1266. doi:10.1016/j.molliq.2016.10.112.

[100] M. Lashkarbolooki, Z. S. Shafipour, A. Z. Hezave, H. Farmani, Use of artificial neural networks for prediction of phase equilibria in the binary system containing carbon dioxide, J. Supercrit. Fluids 75 (2013) 144. doi:10.1016/j.supflu.2012.12.032.

[101] B. Vaferi, Y. Rahnama, P. Darvishi, A. Toorani, M. Lashkarbolooki, Phase equilibria modeling of binary systems containing ethanol using optimal feedforward neural network, J. Supercrit. Fluids 84 (2013) 80. doi:10.1016/j.supflu.2013.09.013.

[102] V. H. Alvarez, M. D. A. Saldaña, Thermodynamic prediction of vapor–liquid equilibrium of supercritical CO_2 or CHF_3+ionic liquids, J. Supercrit. Fluids 66 (2012) 29. doi:10.1016/j.supflu.2012.02.011.

[103] R. V. Vaz, A. L. Magalhães, C. M. Silva, Improved hydrodynamic equations for the accurate prediction of diffusivities in supercritical carbon dioxide, Fluid Phase Equilib. 360 (2013) 401. doi:10.1016/j.fluid.2013.09.052.

[104] J. P. S. Aniceto, B. Zêzere, C. M. Silva, Machine learning models for the prediction of diffusivities in supercritical CO_2 systems, J. Mol. Liq. 326 (2021) 115281. doi:10.1016/j.molliq.2021.115281.

[105] X. Zhao, T. Luo, H. Jin, Predicting diffusion coefficients of binary and ternary supercritical water mixtures *via* machine and transfer learning with deep neural network, Ind. Eng. Chem. Res. 61 (2022) 8542. doi:10.1021/acs.iecr.2c00017.

[106] J. P. S. Aniceto, B. Zêzere, C. M. Silva, Predictive models for the binary diffusion coefficient at infinite dilution in polar and nonpolar fluids, Materials 14 (2021) 542. doi:10.3390/ma14030542.

[107] G. Pan, P. Chen, H. Yan, Y. Lu, A DFT accurate machine learning description of molten $ZnCl_2$ and its mixtures: 1. Potential development and properties prediction of molten $ZnCl_2$, Comput. Mater. Sci. 185 (2020) 109955. doi:10.1016/j.commatsci.2020.109955.

[108] M.-T. Nguyen, R. Rousseau, P. D. Paviet, V.-A. Glezakou, Actinide molten salts: A machine-learning potential molecular dynamics study, ACS Appl. Mater. Interfaces 13 (2021) 53398. doi:10.1021/acsami.1c11358.

[109] G. Sivaraman, J. Guo, L. Ward, N. Hoyt, M. Williamson, I. Foster, C. Benmore, N. E. Jackson, Automated development of molten salt machine learning potentials: Application to LiCl, J. Phys. Chem. Lett. 12 (2021) 4278. doi:10.1021/acs.jpclett.1c00901.

[110] Y. Xie, M. Bu, G. Zou, Y. Zhang, G. Lu, Molecular dynamics simulations of $CaCl_2$–NaCl molten salt based on the machine learn-

ing potentials, Sol. Energy Mater. Sol. Cells 254 (2023) 112275. doi:10.1016/j.solmat.2023.112275.

[111] G. Sivaraman, N. E. Jackson, B. Sanchez-Lengeling, A. Vázquez-Mayagoitia, A. Aspuru-Guzik, V. Vishwanath, J. J. de Pablo, A machine learning workflow for molecular analysis: Application to melting points, Mach. Learn.: Sci. Technol. 1 (2020) 025015. doi:10.1088/2632-2153/ab8aa3.

[112] Z. Acar, P. Nguyen, K. C. Lau, Machine–learning model prediction of ionic liquids melting points, Appl. Sci. 12 (5) (2022) 2408. doi:10.3390/app12052408.

[113] Q.-J. Hong, Melting temperature prediction *via* first principles and deep learning, Comput. Mater. Sci. 214 (2022) 111684. doi:10.1016/j.commatsci.2022.111684.

[114] Q. J. Hong, S. V. Ushakov, A. van de Walle, A. Navrotsky, Melting temperature prediction using a graph neural network model: From ancient minerals to new materials, Proc. Natl. Acad. Sci. USA 119 (2022) e2209630119. doi:10.1073/pnas.2209630119.

[115] D. Saldana, L. Starck, P. Mougin, B. Rousseau, B. Creton, On the rational formulation of alternative fuels: melting point and net heat of combustion predictions for fuel compounds using machine learning methods, SAR QSAR Environ. Res. 24 (2013) 259. doi:10.1080/1062936X.2013.766634.

[116] T. Galeazzo, M. Shiraiwa, Predicting glass transition temperature and melting point of organic compounds *via* machine learning and molecular embeddings, Environ. Sci. Atmos. 2 (3) (2022) 362. doi:10.1039/D1EA00090J.

[117] V. Venkatraman, S. Evjen, H. K. Knuutila, A. Fiksdahl, B. K. Alsberg, Predicting ionic liquid melting points using machine learning, J. Mol. Liq. 264 (2018) 318. doi:10.1016/j.molliq.2018.03.090.

[118] K. Low, R. Kobayashi, E. I. Izgorodina, The effect of descriptor choice in machine learning models for ionic liquid melting point prediction, J. Chem. Phys. 153 (2020) 104101. doi:10.1063/5.0016289.

[119] R. S. M. Freitas, A. P. F. Lima, C. Chen, F. A. Rochinha, D. Mira, X. Jiang, Towards predicting liquid fuel physicochemical properties using molecular dynamics guided machine learning models, Fuel 329 (2022) 125415. doi:10.1016/j.fuel.2022.125415.

[120] Y. Chen, X. Liang, J. M. Woodley, G. M. Kontogeorgis, Modelling study on phase equilibria behavior of ionic liquid–based aqueous biphasic systems, Chem. Eng. Sci. 247 (2022) 116904. doi:10.1016/j.ces.2021.116904.

[121] G. Sun, Z. Zhao, S. Sun, Y. Ma, H. Li, X. Gao, Vapor–liquid phase equilibria behavior prediction of binary mixtures using machine learning, Chem. Eng. Sci. 282 (2023) 119358. doi:10.1016/j.ces.2023.119358.

[122] M. Hosseini, Y. Leonenko, Development of explicit models to predict methane hydrate equilibrium conditions in pure water and brine solutions: A machine learning approach, Chem. Eng. Sci. (2023) 119603doi:10.1016/j.ces.2023.119603.

[123] C. J. Barton, J. P. Blakely, K. A. Allen, W. C. Davis, B. S. Weaver, The system LiOH-NaOH, in: R. E. Thoma (Ed.), Phase Diagrams of Nuclear Reactor Materials, 15th Edition, Vol. ORNL-2548, Oak Ridge National Laboratory, Oak Ridge, TN, 1959, p. 140. doi:10.2172/4234144.

[124] R. Cohen-Adad, A. Tranquard, R. Péronne, P. Negri, A.-P. Rollet, Le système eau-hydroxyde de sodium, C. R. Acad. Sci. 251 (1960) 2035, gallica.bnf.fr/ark:/12148/bpt6k7614/f93.item.

[125] Y. M. Baikov, Ionic motion in various forms of solid-state alkali-metal hydroxides: Individual compounds, eutectic mixtures, and crystalline hydrates, Solid State Ionics 208 (2012) 17. doi:10.1016/j.ssi.2011.11.033.

[126] R. Cohen-Adad, M. Michaud, Les équilibres liquide–solide du système binaire eau–potasse, C. R. Acad. Sci. 242 (1956) 2569, gallica.bnf.fr/ark:/12148/bpt6k6936/f799.item.

[127] G. von Hevesy, Über Alkalihydroxyde. L: Die Zweistoffsysteme Natriumhydroxyd—Kaliumhydroxyd, Kaliumhydroxyd—Rubidiumhydroxyd und Rubidiumhydroxyd—Natriumhydroxyd, Z. Phys. Chem. 73U (1910) 667. doi:10.1515/zpch-1910-7336.

[128] A. Kacprzak, R. Kobylecki, Z. Bis, Influence of temperature and composition of NaOH–KOH and NaOH–LiOH electrolytes on the performance of a direct carbon fuel cell, J. Power Sources 239 (2013) 409. doi:10.1016/j.jpowsour.2013.03.159.

[129] M. Michaud, Étude du systeme binaire potasse-lithine, C. R. Hebd. Seances Acad. Sci. C 264 (1967) 1939, gallica.bnf.fr/ark:/12148/bpt6k62157799.

[130] M. Michaud, Contribution á l'étude des hydroxydes de potassium et de baryum, Rev. Chim. Minér. 5 (1968) 89.

[131] E. F. Stephan, P. D. Miller, Solubility of lithium hydroxide in water and vapor pressure of solutions above 220 °F, J. Chem. Eng. Data 7 (1962) 501. doi:10.1021/je60015a018.

[132] H. W. Otto, R. P. Seward, Phase equilibria in the potassium hydroxide–sodium hydroxide system., J. Chem. Eng. Data 9 (1964) 507. doi:10.1021/je60023a009.

[133] A.-P. Rollet, R. Cohen-Adad, J. Choucroun, Préparation d'hydroxydes alcalins anhydres exempts de carbonates, J., Bull. Soc. Chim. France 1 (1959) 146.

[134] W. J. Smothers, R. F. Kruh, J. K. Carlton, Y. Chiang, A study of phase transitions in sodium hydroxide, J. Appl. Chem. 4 (1954) 268. doi:10.1002/jctb.5010040505.

[135] Y. Takahashi, M. Kamimoto, R. Sakamoto, K. Kanari, T. Ozawa, Thermoanalytical evaluation of eutectic mixtures of LiOH, NaOH and KOH for latent heat thermal energy storage, Nippon Kagaku Kaishi 1982 (6) (1982) 1049. doi:10.1246/nikkashi.1982.1049.

[136] S. Dai, L. Liu, H. He, B. Yang, D. Wu, Y. Zhao, D. Niu, Highly–efficient molten NaOH-KOH for organochlorine destruction: Performance and mechanism, Environ. Res. 217 (2023) 114815. doi:10.1016/j.envres.2022.114815.

[137] G. Scarpa, Analisi termica delle miscele degli idrati alcalini coi corrispondenti alogenuri. I. Composti di litio, Atti Accad. Lincei 24 (2) (1915) 476, biodiversitylibrary.org/item/155367.

[138] G. Scarpa, Analisi termica delle miscele degli idrati alcalini coi corrispondenti alogenuri. I. Composti di potassio, Atti Accad. Lincei 24 (1) (1915) 738, biodiversitylibrary.org/item/155367.

[139] G. Scarpa, Analisi termica delle miscele degli idrati alcalini coi corrispondenti alogenuri. I. Composti di sodio, Atti Accad. Lincei 24 (1) (1915) 955, biodiversitylibrary.org/item/155367.

[140] F. Pedregosa, G. Varoquaux, A. Gramfort, V. Michel, B. Thirion, O. Grisel, M. Blondel, P. Prettenhofer, R. Weiss, V. Dubourg, J. Vanderplas, A. Passos, D. Cournapeau, M. Brucher, M. Perrot, E. Duchesnay, Scikit–learn: Machine learning in python, J. Mach. Learn. Res. 12 (2011) 2825, jmlr.org/papers/v12/pedregosa11a.html.

[141] F. Perez, B. E. Granger, iPython: A system for interactive scientific computing, Comput. Sci. Eng. 9 (2007) 21. doi:10.1109/MCSE.2007.53.

[142] Y. Dessureault, J. Sangster, A. D. Pelton, Coupled phase diagram - Thermodynamic analysis of the 24 binary systems, A_2CO_3-AX and A_2SO_4-AX Where A = Li, Na, K and X = Cl, F, NO_3, OH, J. Phys. Chem. Ref. Data 19 (1990) 1149. doi:10.1063/1.555866.